RSC Advances

This is an *Accepted Manuscript*, which has been through the Royal Society of Chemistry peer review process and has been accepted for publication.

Accepted Manuscripts are published online shortly after acceptance, before technical editing, formatting and proof reading. Using this free service, authors can make their results available to the community, in citable form, before we publish the edited article. This *Accepted Manuscript* will be replaced by the edited, formatted and paginated article as soon as this is available.

You can find more information about *Accepted Manuscripts* in the Information for Authors.

Please note that technical editing may introduce minor changes to the text and/or graphics, which may alter content. The journal's standard Terms & Conditions and the Ethical guidelines still apply. In no event shall the Royal Society of Chemistry be held responsible for any errors or omissions in this *Accepted Manuscript* or any consequences arising from the use of any information it contains.

ROYAL SOCIETY OF CHEMISTRY

www.rsc.org/advances

Please do not adjust margins

RSC Advances

Paper

Capacitance enhancement by electrochemically active benzene derivatives for graphene-based supercapacitors†

Received 00th January 20xx,
Accepted 00th January 20xx

DOI: 10.1039/x0xx00000x

www.rsc.org/

Zhen-Kun Wu,[ab] Ziyin Lin,[b] Liyi Li,[b] Bo Song,[b] Chia-Chi Tuan,[b] Zhuo Li,[b] Kyoung-sik Moon,[b] Shu-Lin Bai*[a] and Ching-Ping Wong*[bc]

Various aromatic molecules have been reported to improve the performance of reduced graphene oxide (rGO)-based supercapacitors. However, the mechanism for this improvement remains unclear. Here we design a facile approach that clearly identifies the main reason for the enhancement. Benzene derivatives, namely *p*-phenylenediamine (PPD), *m*-phenylenediamine (MPD), *o*-phenylenediamine (OPD), hydroquinone (HQ), phenol, aniline and *p*-aminophenol (PAP) are incorporated into graphene oxide (GO) layers during their reduction and assembly at room temperature. We find that the capacitance increase mainly arises from the pseudocapacitance of specific benzene derivative molecules rather than their spacing effect. Moreover, the *para* and *ortho* substituted benzene derivatives contribute much more than the meta substituted ones do. With a small amount of PPD (~11 wt%), the specific capacitance reaches 273 F/g, much higher than that of pure rGO electrodes (113 F/g). The hybrid electrode also shows great stability with a capacitance retention of up to 86% after 10000 charge/discharge cycles.

1 Introduction

Supercapacitors have been considered as a promising energy storage unit for portable electronics, electric vehicles, *etc.* due to their high power density and long lifetime.[1] Various materials have been investigated as the active electrode, such as metal oxides,[2,3] conducting polymers,[4,5] activated carbon (AC),[6] carbon nanotubes (CNTs),[7] graphene derivatives[8,9] as well as the hybrids of these materials.[3,10] Among all these materials, reduced graphene oxide (rGO) is most extensively studied because of its extremely high specific surface area, good electrical conductivity and the capability for mass production.[11,12] However, the specific capacitance reported for graphene (~ 100 to 200 F/g) is much smaller than the theoretical value (~550 F/g).[13] This deficiency largely results from the aggregation of graphene sheets caused by the Van der Waals force, which greatly reduces the surface area accessible to the electrolyte and thus decreases the specific capacitance.

Generally two approaches have been used to improve the capacitance performance of graphene-based materials. The first one is through the modification of rGO morphology to increase the surface area accessible to the electrolyte. For example, curved graphene that alleviates the aggregation during sample preparation was prepared by anti-solvent[14] or fast-solvent-evaporation treatment.[15] In addition, different types of spacers, such as $Mg(OH)_2$,[16] CNTs[17] and covalently-grafted benzene molecules[18] were introduced to increase the spacing between the rGO sheets. Specific capacitances ranging from 150 to 450 F/g are achieved by these methods. The second approach is the incorporation of electrochemically active materials that can provide large pseudocapacitance via rapid redox reactions, such as metal oxides,[2,3] conducting polymers[4,5] and small aromatic chemicals.[19-21] Among these materials, electrochemically active benzene derivatives have attracted a lot of attentions. For example, Xu et al. incorporated hydroquinone (HQ) and achieved a specific capacitance of 441 F/g.[19] Lu et al. reported a specific capacitance of 313 F/g with *p*-phenylenediamine (PPD)/rGO hybrid electrode, of which the improvement was attributed to spacing and nitrogen doping effect.[20] Cui et al. investigated *1,2,4,5*-benzenetetraamine grafted rGO and obtained a specific capacitance of 370 F/g.[21] These benzene derivatives are very promising because of their large capacitance and ease of mass production. However, the roles these benzene derivatives play remain unclear. The puzzle becomes more complicated when the reactions occur at high temperatures that may introduce by-products into the system.[19-22]

Herein we design a facile approach to study the capacitance contribution from electrochemically active benzene derivatives. In this work, GO is mixed with a specific benzene derivative, after which it is simultaneously reduced and assembled with a zinc plate at room temperature. The benzene derivative molecules are physically adsorbed on the

[a] Department of Materials Science and Engineering, HEDPS/CAPT/LTCS, College of Engineering, Peking University Beijing 100871, P. R. China. E-mail: slbai@pku.edu.cn
[b] School of Material Science and Engineering, Georgia Institute of Technology, Atlanta, GA 30332, United States. E-mail:cp.wong@mse.gatech.edu
[c] College of Engineering, The Chinese University of Hong Kong, Hong Kong
Electronic Supplementary Information (ESI) available: See
DOI: 10.1039/x0xx00000x

RSC Advances Accepted Manuscript

Please do not adjust margins

rGO layers in a face-to-face fashion via π-π interaction. The solid phase and room temperature reduction of GO avoids the side reactions that may occur at elevated temperatures. Moreover, the interaction

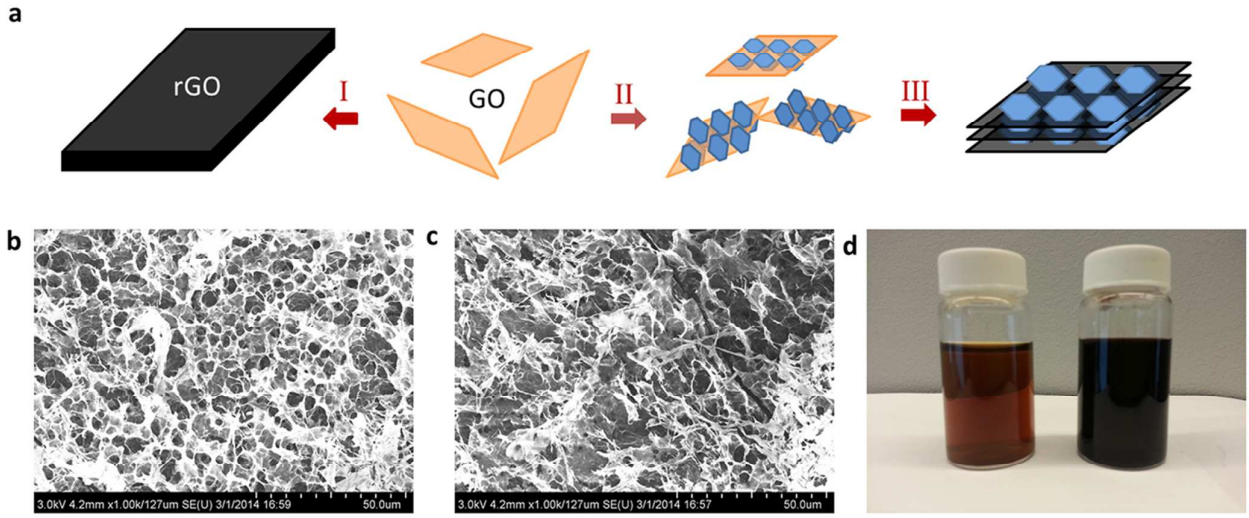

Fig. 1(a) Schematic illustration of the fabrication of rGO and *p*-rGO. I) GO is reduced into rGO with zinc plate; II) GO is mixed with PPD; III) GO/PPD mixture is reduced into *p*-rGO with a zinc plate. (b,c) SEM images of freeze-dried rGO and *p*-rGO aerogels, respectively. (d) Left: GO solution; right: GO/PPD solution. Both samples were left for one day before the images were taken.

between benzene derivatives and rGO is non-covalent, which helps to separate the contributions from spacing effect and pseudocapacitance effect. By investigating the performance a series of similar benzene derivatives/rGO electrodes (*b*-rGO, in which *b*- stands for benzene derivatives including phenol, aniline, HQ, *p*-aminophenol (PAP), *o*-phenylenediamine (OPD), and *m*-phenylenediamine (MPD)), we find that the capacitance increase mainly arises from the pseudocapacitance of specific benzene derivative molecules rather than their spacing effect. With a small loading of PPD, a specific capacitance of 273 F/g and a capacitance retention of 86% after 10000 charge/discharge cycles are achieved.

2 Experimental

2.1 Reagents, materials and synthesis

All chemicals used in this work were used as received without any further purification. GO was synthesized according to a modified Hummers' method.[23,24] Briefly, $NaNO_3$ (4 g) was dissolved into concentrated H_2SO_4 (98 wt%, 200 mL) in an ice bath. Graphite powder (Asbury 230U, 4 g) and $KMnO_4$ (18 g) were added into the solution slowly with the temperature kept below 8 °C. The mixture was vigorously stirred for 2 h in the ice bath and another 30 min in a 35 °C water bath. After the reaction, the solution was diluted with deionized water (500 mL) followed by the addition of H_2O_2 (30% w/w in H_2O, 50 mL), during which the temperature was maintained below 80 °C. The as-obtained GO was washed with HCl (1 M, 2 L) and deionized water until the pH reached 6.

GO (1 mg/mL, 40 mL) was first dispersed in water and ultrasonically exfoliated for 30 min. Benzene derivative such as phenol, aniline, HQ and PAP, OPD or MPD (0.36 mM if not stated otherwise) was added into the solution and ultrasonicated for another 30 min. In this process the aromatic molecules dissolved in the GO solution and attached onto the GO surface. After that a Zn plate (4 cm × 4 cm) was immersed in the GO solution at ambient temperature, during which GO was reduced into rGO hydrogel. The as-prepared *b*-rGO hydrogel film was removed from the substrate by immersion in a dilute HCl solution for about 30 min. Then it was washed with excess dilute HCl for 1 h and 10 L deionized water for two days to remove the Zn residues and non-adsorbed aromatic molecules.

2.2 Characterization

The morphologies of GO, rGO and PPD/rGO (*p*-rGO) were characterized with scanning electron microscope (SEM, Hitachi SU8010) and atomic force microscope (AFM, Dimension Edge, Veeco with silicon tip MPP-11100-10). Raman spectra were taken with LabRAM ARAMIS, HORIBA JOBIN YVON using 532 nm laser as the excitation light. X-ray photoelectron spectrum (XPS) measurement was performed with a Thermo K-Alpha XPS. Fourier transform infrared spectrum (FTIR) was obtained with FTIR spectrometer (Nicolet, Magna IR 560) at room temperature. X-ray diffraction (XRD) was performed with an X'Pert Pro Alpha-1 machine with Cu Kα radiation.

2.3 Electrochemical Measurements

Two-electrode and three-electrode test setups were used to test the electrochemical performance. For the two-electrode test setup, a regular filter paper was sandwiched between two circular hydrogels as the separator (Φ=1.0 cm, loading ~ 1 mg/cm^2). The sandwiched structure was kept between two stainless steel plates that serve as the current collector. For the three-electrode test setup, a platinum wire and Ag/AgCl

RSC Advances Accepted Manuscript

 This journal is © The Royal Society of Chemistry 2015

electrode filled with saturated KCl aqueous solution were used as the counter and reference electrode, respectively. A rectangular hydrogel (0.5 cm × 2 cm) was pressed onto a gold foil with a piece of carbon fibre paper to improve the contact between the hydrogel and the gold current collector. 1 M H_2SO_4 was used as the electrolyte throughout this work. Before test, the samples were soaked into the electrolyte for 3 h. Cyclic voltammetry (CV), galvanostatic charge/discharge test (CD) and electrochemical impedance spectroscopy (EIS) were carried out with a Versastat 2-channel system (Princeton Applied Research). EIS was carried out in the frequency range of 0.01 Hz to 100 kHz with a 10 mV sinusoidal voltage.

3 Results and Discussion

3.1 The reduction process

The reduction process is illustrated in Fig. 1a. Active metals such as zinc, iron and copper can reduce GO at ambient temperature due to their lower redox potentials.[25,26] Here Zn plate is used as the reducing agent and PPD is used as a representative of these benzene derivatives. Due to its higher redox potential, the GO sheet will be spontaneously reduced once it contacts with the Zn plate. The as-reduced rGO is electrically conductive, which in turn serves as the electron conducting path for the continuous reduction and assembly of GO sheets. The SEM images of rGO (Fig. 1b) and *p*-rGO (Fig. 1c) exhibit a similar open-porous structure that reflects the layer-by-layer reducing mechanism. In addition, it also helps the ion transport within the electrode, which is beneficial for the electrochemical performance.[26] This simple reducing method takes place at room temperature and uses solid phase reducing agent. As a result, it avoids the side reactions that may occur at elevated temperatures or by using liquid reducing agents, making it excellent to study the function of these benzene derivatives.[22] Fig. 1d presents the photos of 1 mg/mL GO solution with (right) and without (left) the addition of PPD. Both samples had been left for 24 h before these photos were taken and neither of them showed any sign of agglomeration. The stable dispersion arises from the electric repulsion between the negatively charged GO sheets in water.[27] Meanwhile, the addition of PPD does not disturb the stability, indicating PPD does not interact with rGO electrostatically.

The morphology of GO and rGO after the PPD absorption is characterized by AFM and XRD, respectively. From the AFM images, the thickness of GO is 0.9 nm (Fig. 2a) and this value increases to 1.6 nm after the PPD attachment to GO (Fig. 2b).

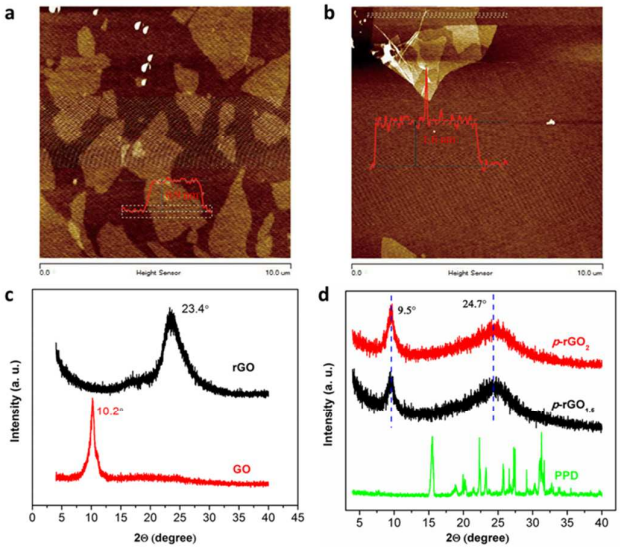

Fig. 2 (a,b) AFM images of GO and PPD/GO, respectively. (c) XRD patterns of GO and rGO. (d) XRD patterns of PPD and *p*-rGO. The subscript designates the weight ratio of PPD to GO.

Fig. 2c shows the XRD patterns of GO and rGO reduced with Zn plate. A sharp peak appears at 10.2° for GO, corresponding to an inter-layer spacing of 0.87 nm. The peak shifts to 23.4° after reduction, which corresponds to an inter-layer spacing of 0.38nm. For p-rGO, a distinct new peak shows up at 9.5°, which does not exist in the XRD patterns of neither rGO nor PPD (Fig. 2d). This peak corresponds to a spacing of 0.93 nm, 0.57 nm larger than that of the graphitic peak (0.36nm). The height increase from AFM and XRD characterization is equivalent to twice the thickness of the aromatic core.[5,28] It thus indicates that the PPD molecules may attach parallel onto both sides of GO surfaces. The small difference between PPD/GO (0.7 nm) and *p*-rGO (0.57nm) can be attributed to the restoration of π-conjugation and the accompanied stronger interaction between rGO and PPD molecules.

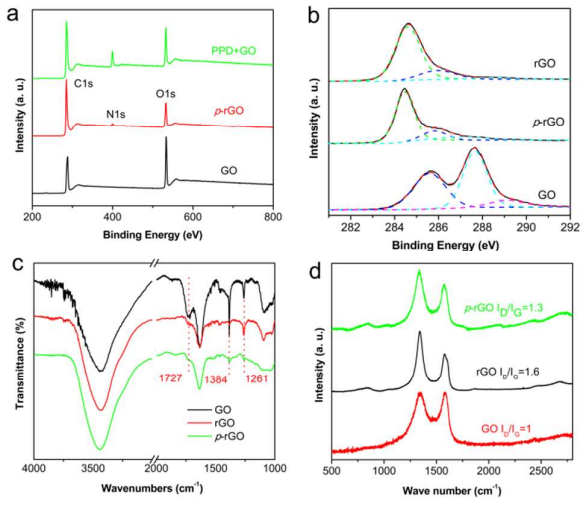

Fig. 3 (a) XPS survey spectra of GO, *p*-rGO and PPD/GO. (b) C1s spectra of GO, rGO and *p*-rGO. (c) FTIR spectra of GO, rGO and *p*-rGO. (d) Raman spectra of GO, rGO and *p*-rGO.

RSC Advances Accepted Manuscript

The interaction between PPD and rGO is proved to be non-covalent by chemical analysis. The XPS survey of p-rGO shows a small N1s peak from the residue of PPD molecules at 400 eV (Fig. 3a). It thus proves the existence of PPD molecules even after prolonged washing. The strong adsorption should arise from the interaction between graphene and the benzene derivatives. The deconvoluted N1s spectrum (Fig. S1) contains a single peak centred at 399.5 eV, corresponding to the amine group in PPD.[29] Neither pyridinic nitrogen (398.2 eV) nor graphitic nitrogen (401.3 eV) shows up in the spectrum.[18,29] Fig. 3b presents the deconvoluted C1s XPS spectra for GO, rGO and *p*-rGO. The rGO shows three distinct peaks at 284.6 eV, 286.0 eV and 288.5 eV, corresponding to C-C, C-O and C=O bonds, respectively. The C-O peak intensity of GO sharply decreases after it is reduced by Zn. In addition, the C/O ratio from survey spectra increases from 2.4 for GO to 6.4 for rGO and 5.2 for *p*-rGO, suggesting an efficient removal of oxygen during the process. The similar C/O ratio found in rGO and *p*-rGO indicates that the addition of PPD does not affect the reduction process significantly. Fig. 3c shows the FTIR spectra of GO, rGO and *p*-rGO. The peak intensities at 1727 cm^{-1} (C=O), 1384 cm^{-1} (O-H) and 1261 cm^{-1} (epoxy group)[29] for rGO and *p*-rGO are significantly smaller than those of GO, which also proves the successful reduction. The spectrum of *p*-rGO is nearly identical to that of rGO reduced by Zn. It thus implies that the PPD molecules do not react with GO or rGO in the presence of Zn at room temperature. As a comparison, a control sample is prepared by hydrothermal treatment of GO with the addition of PPD. A distinct new peak at 1567 cm^{-1} appears in the FTIR spectrum, corresponding to the formation of a new N-H bending vibration that does not exist in *p*-rGO or PPD itself (Fig. S2).[16,18] It means that the hydrothermal method will generate new products while our room temperature reduction with Zn plate won't. The Raman spectra of GO, rGO and *p*-rGO (in Fig. 3d) show two characteristic peaks at 1342 cm^{-1} and 1577 cm^{-1},

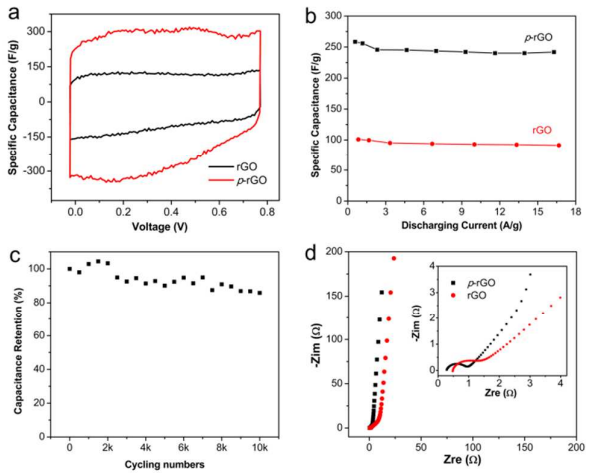

Fig. 4 Electrochemical performance of the rGO and *p*-rGO electrodes in 1 M H_2SO_4 aqueous electrolyte. (a) CV curves of rGO and *p*-rGO at a scan rate of 2 mV/s. (b) Specific capacitance of rGO and *p*-rGO at different current densities. (c) Cycling stability of *p*-rGO electrode at a current density of 11.9 A/g. (d) Impedance spectra of rGO and *p*-rGO. The inset shows the part of spectra at high frequency region.

corresponding to D and G bands of graphene, respectively. The I_D/I_G ratio increases from 1 of GO to 1.6 and 1.3 for rGO and *p*-rGO after the Zn-assisted reduction. The increase can be attributed to the restoration of small graphene domains, a widely observed phenomenon for GO reduction.[30] In conclusion, these characterizations reveal that the PPD molecules remain after the reduction and washing process, during which they do not react with the GO or rGO.

From the characterizations above, we find that PPD is adsorbed parallel to rGO sheets via a non-covalent interaction. We propose this adsorption arises from π-π interaction, which is supported with our characterization and other similar reported experiments.[19,31] It also agrees well with theoretically demonstration that graphene interacts with benzene or other similar π-conjugated molecules via π-π interaction and amino/hydroxyl substitution will increase this interaction.[5,32] Meanwhile, the PPD/GO dispersion in water is very stable, which is opposite to the rapid agglomeration caused by the electric attraction between oppositely charged materials.[16] As a result, the electric interaction is also excluded in our case.

3.2 Electrochemical test of rGO and p-rGO

Electrochemical characterizations are carried out with a two-electrode test setup.[33] Fig. 4a shows the CV curves for rGO and *p*-rGO at a scan rate of 2 mV/s. The specific capacitance calculated based on the CV curves increases from 113 F/g for rGO to 273 F/g for *p*-rGO. Fig. S3 represents the CD plots of *p*-rGO at different current density. The linear and symmetric CD curves give a Coulombic efficiency of 97.5% and indicate excellent charge storage reversibility. In addition, the *p*-rGO exhibits excellent rate performance. The capacitance at a discharge current density of 16 A/g is 242 F/g, which retains 93.6% of the value (259 F/g) at 0.6 A/g (Fig. 4b). The superior rate behaviour can be attributed to the conductive open-porous rGO hydrogel structure as well as the extremely short electron path of the face-to-face attaching mechanism. The hybrid electrode also shows excellent stability; it retains 86% of the initial capacitance after 10000 cycles in the CD test at a current density of 11.9 A/g (Fig. 4c). This capacitance retention is much better compared to those materials composed of metal oxides (84% after 1,000 cycles)[3] and conducting polymers (70% after 1,000 cycles).[4] The impedance spectroscopy is also tested for rGO and *p*-rGO (Fig. 4d). Both spectra are nearly vertical to the real axis at the low frequency region, which indicates pure capacitive behaviour and confirms excellent ion transport within the electrode materials.[6,26] The electrochemical series

RSC Advances Accepted Manuscript

This journal is © The Royal Society of Chemistry 2015

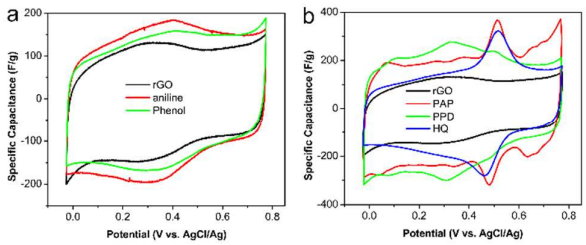

Fig. 5 CV curves of (a) rGO, aniline-rGO, phenol-rGO and (b) rGO, *p*-rGO, *PAP*-rGO and *HQ*-rGO at a scan rate of 10 mV/s in 1 M H_2SO_4 aqueous electrolyte.

resistance, estimated from the intercept of the impedance spectrum at low frequency region with the real axis, is comparable for rGO (4.1 Ω) and *p*-rGO (3.0 Ω). At high frequencies, there's a loop corresponding to a nano-porous structure within both rGO and *p*-rGO.[6] The small internal resistance for *p*-rGO (0.28 Ω) also confirms the excellent electrical conductivity with the presence of PPD.

3.3 Mechanism study

In order to understand the role of benzene derivatives in the capacitance enhancement, a series of benzene derivatives are incorporated into rGO following the same procedure as p-rGO. Their specific capacitances are measured using a three-electrode setup in which the redox reactions can be closely monitored by the corresponding pseudocapacitive CV peaks.

We firstly compared *mono*-substituted benzene (phenol and aniline) and *bi*-substituted benzene (HQ, PAP and PPD). All of these aromatic molecules improve the specific capacitance to some extent. However, the CV curves for *mono*-substituted benzene treated rGO (*mono*-rGO) show similar shapes and areas to that of rGO (Fig. 5a); whereas those for *bi*-substituted benzene treated rGO (*bi*-rGO) exhibit new pseudocapacitive peaks (Fig. 5b). The specific capacitance are 143, 128, 210, 160 and 211 F/g for as-prepared electrodes incorporated with aniline, phenol, PPD, HQ and PAP, respectively. The capacitance enhancement with *mono* molecules is generally less than 30 F/g from that of rGO (115 F/g), while those for *bi*-rGOs are much larger (~100 F/g).

Mono- and *bi*-substituted benzenes have similar chemical structures with an aromatic core in the center that provides the adsorption force onto the graphene sheets. As a result, the specific capacitance for *mono*-rGO and *bi*-rGO should be comparable if the enhancement primarily comes from the spacing effect of the aromatic core. However, this expectation is in contradictory to the actual measurement with much smaller enhancements for *mono*-rGOs than for *bi*-rGOs. Moreover, peaks corresponding to redox reactions show up in the CV curves for *bi*-rGOs, indicating the occurrence of redox reactions. Therefore, we believe that these redox reactions, which only occur when two functional groups are present in a benzene ring, are the major contributors for the large enhancement of bi-rGOs' specific capacitance. We suggest that the capacitance increase primarily results from redox reactions similar to the one between quinone and hydroquinone.[34]

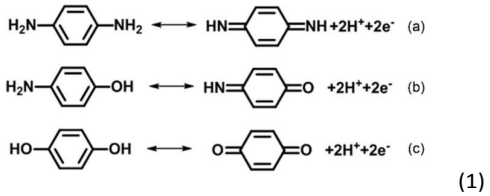

(1)

If the mechanism proposed above stands, there should be some differences among *bi*-substituted benzene derivatives with different configurations. For example, like PPD, redox reaction occurs between OPD and *o*-benzoquinone diimine

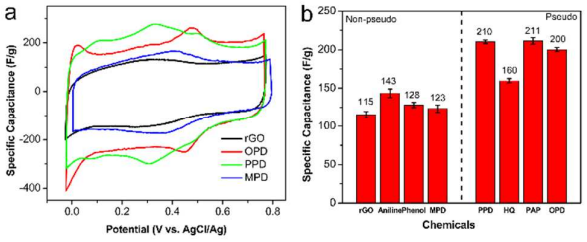

Fig. 6 (a) CV curves of rGO, *p*-rGO, *m*-rGO and *o*-rGO at a scan rate of 10 mV/s 1 M H_2SO_4 aqueous electrolyte. (b) Specific capacitance histogram of rGO, *mono*-rGOs and *bi*-rGOs.

(OBD). However, there is no similar reaction for MPD. As a result, it is expected that MPD will not result in capacitance enhancement from the pseudocapacitance effect. Indeed, from the CV measurements, distinct redox reaction peaks do show up at about 0.5 V for OPD/rGO (*o*-rGO). However, no such peaks appear for MPD/rGO (*m*-rGO, Fig. 6a). The specific capacitance of *o*-rGO (200 F/g) is much larger than that of *m*-rGO (123 F/g), which agrees well with the proposed mechanism. Based on these findings, we can conclude that the main reason for the capacitance increase is the redox reactions from the benzene derivatives with *para* and *ortho* configurations of amino or hydroxyl groups.

The specific capacitance is listed in Fig. 6b. It is obvious that the specific capacitances for samples without redox reactions (on the left) are much lower than those with (on the right). In addition, the above-mentioned hypothesis is further supported with the calculated results. The atom ratio of C/O/N for *p*-rGO is 82.8:14.3:2.9 obtained from the XPS survey spectrum, from which the PPD loading after reduction is estimated to be about 11 wt% (see Supplementary Methods). Assuming the capacitance contribution from rGO remains unchanged in *p*-rGO, the expected specific capacitance of *p*-rGO is about 299 F/g. This value agrees well with the measurement value of 273 F/g. Moreover, the specific capacitance contributed by PPD alone is about 1551 F/g, which is 87% of its theoretical value (1784 F/g derived from Reaction 1(a)). The supreme utilization may have aroused from the double-sided parallel adsorption mechanism that guarantees excellent contact between rGO and the pseudocapacitive molecules.

RSC Advances Accepted Manuscript

4 Conclusions

In summary, PPD is incorporated into rGO and significantly increases the specific capacitance. The as-fabricated *p*-rGO also exhibits excellent rate capability and cycling performance. After investigating a series of benzene derivatives, the main reason for the capacitance improvement is clearly attributed to the pseudocapacitance of the aromatic molecules themselves rather than the spacing effect. The pseudocapacitance arises from the redox reactions of the molecules. In accordance, the configuration of functional groups plays an important role in the capacitive enhancement; *para* and *ortho* substituted benzene derivatives have much higher capacitance values than that obtained with *meta* substituted ones. This conclusion will guide the searching of promising aromatic molecules for further enhanced supercapacitors.

Acknowledgements

This work was partially supported by Advanced Research Project Agency- Energy (ARPA-E) program # DE-AR0000303 and the National Natural Science Foundation of China (Nos. 11272008 and 11361161001). Chinese Scholarship Council financially supported Zhenkun Wu in participating GT-PKU Joint Ph.D. Program during his study in the United States.

Notes and references

1 P. Thounthong, S. Rael and B. Davat, *J. Power Sources*, 2009, **193**, 376-385.
2 W. Wei, X. Cui, W. Chen and D. G. Ivey, *Chem. Soc. Rev.*, 2011, **40**, 1697-1721.
3 S. Chen, J. Zhu, X. Wu, Q. Han and X. Wang, *ACS nano*, 2010, **4**, 2822-2830.
4 K. Zhang, L. L. Zhang, X. Zhao and J. Wu, *Chem. Mater.*, 2010, **22**, 1392-1401.
5 J. D. Wuest and A. Rochefort, *Chem. Commun.*, 2010, **46**, 2923-2925.
6 J. Gamby, P. Taberna, P. Simon, J. Fauvarque and M. Chesneau, *J. Power Sources*, 2001, **101**, 109-116.
7 K. H. An, W. S. Kim, Y. S. Park, J.-M. Moon, D. J. Bae, S. C. Lim, Y. S. Lee and Y. H. Lee, *Adv. Funct. Mater.* , 2001, **11**, 387-392.
8 Z. Lin, Y. Liu, Y. Yao, O. J. Hildreth, Z. Li, K. Moon and C.-p. Wong, *J. Phys. Chem. C*, 2011, **115**, 7120-7125.
9 H. Ji, X. Zhao, Z. Qiao, J. Jung, Y. Zhu, Y. Lu, L. L. Zhang, A. H. MacDonald and R. S. Ruoff, *Nat. Commun.*, 2014, **5**, 4317.
10 D. Yu and L. Dai, *J. Phys. Chem. Lett.* , 2009, **1**, 467-470.
11 Y. Wang, Z. Shi, Y. Huang, Y. Ma, C. Wang, M. Chen and Y. Chen, *J. Phys. Chem. C*, 2009, **113**, 13103-13107.
12 Y. Zhu, S. Murali, M. D. Stoller, K. Ganesh, W. Cai, P. J. Ferreira, A. Pirkle, R. M. Wallace, K. A. Cychosz and M. Thommes, *Science*, 2011, **332**, 1537-1541.
13 M. D. Stoller, S. Park, Y. Zhu, J. An and R. S. Ruoff, *Nano Lett.*, 2008, **8**, 3498-3502.
14 Y. Yoon, K. Lee, C. Baik, H. Yoo, M. Min, Y. Park, S. M. Lee and H. Lee, *Adv. Mater.*, 2013, **25**, 4437-4444.
15 C. Liu, Z. Yu, D. Neff, A. Zhamu and B. Z. Jang, *Nano Lett.*, 2010, **10**, 4863-4868.
16 J. Yan, Q. Wang, T. Wei, L. Jiang, M. Zhang, X. Jing and Z. Fan, *ACS nano*, 2014, **8**, 4720-4729.
17 Q. Cheng, J. Tang, J. Ma, H. Zhang, N. Shinya and L.-C. Qin, *Phys. Chem. Chem. Phys.*, 2011, **13**, 17615-17624.
18 H. Li, Y. Wang, Y. Shi, J. Li, L. He and H. Y. Yang, *RSC Adv.*, 2013, **3**, 14954-14959.
19 Y. Xu, Z. Lin, X. Huang, Y. Wang, Y. Huang and X. Duan, *Adv. Mater.*, 2013, **25**, 5779-5784.
20 Y. Lu, Y. Huang, F. Zhang, L. Zhang, X. Yang, T. Zhang, K. Leng, M. Zhang and Y. Chen, *Chinese Sci. Bull.*, 2014, **59**, 1809-1815.
21 Y. Cui, Q.-Y. Cheng, H. Wu, Z. Wei and B.-H. Han, *Nanoscale*, 2013, **5**, 8367-8374.
22 Y. Chen, X. Zhang, P. Yu and Y. Ma, *Chem. Commun.*, 2009, 4527-4529.
23 W. S. Hummers Jr and R. E. Offeman, *J. Am. Chem. Soc.*, 1958, **80**, 1339-1339.
24 Z.-K. Wu, Z. Lin, L. Li, B. Song, K.-s. Moon, S.-L. Bai and C.-P. Wong, *Nano Energy*, 2014, **10**, 222-228.
25 X. Cao, D. Qi, S. Yin, J. Bu, F. Li, C. F. Goh, S. Zhang and X. Chen, *Adv. Mater.*, 2013, **25**, 2957-2962.
26 U. N. Maiti, J. Lim, K. E. Lee, W. J. Lee and S. O. Kim, *Adv. Mater.*, 2014, **26**, 615-619.
27 D. Li, M. B. Müller, S. Gilje, R. B. Kaner and G. G. Wallace, *Nat. Nanotechnol.*, 2008, **3**, 101-105.
28 Y. Xu, H. Bai, G. Lu, C. Li and G. Shi, *J. Am. Chem. Soc.*, 2008, **130**, 5856-5857.
29 O. C. Compton, D. A. Dikin, K. W. Putz, L. C. Brinson and S. T. Nguyen, *Adv. Mater.*, 2010, **22**, 892-896.
30 H. Wang, J. T. Robinson, X. Li and H. Dai, *J. Am. Chem. Soc.*, 2009, **131**, 9910-9911.
31 T. Xue, S. Jiang, Y. Qu, Q. Su, R. Cheng, S. Dubin, C. Y. Chiu, R. Kaner, Y. Huang and X. Duan, *Angewandte Chemie*, 2012, **124**, 3888-3891.
32 A. Rochefort and J. D. Wuest, *Langmuir*, 2008, **25**, 210-215.
33 M. D. Stoller and R. S. Ruoff, *Energ. Environ. Sci.*, 2010, **3**, 1294-1301.
34 L. Duić and S. Grigić, *Electrochim. Acta*, 2001, **46**, 2795-2803.

RSC Advances Accepted Manuscript

 This journal is © The Royal Society of Chemistry 2015